CYBERNETICS AND PHYSICS, VOL. 12, NO. 4, 2023, 264–274

SUITABILITY OF DIFFERENT MACHINE LEARNING METHODS FOR HIGH-SPEED FLOW MODELLING ISSUES

Vladimir A. Istomin
Saint Petersburg State University
Saint Petersburg
Russian Federation
v.istomin@spbu.ru

Semen A. Pavlov
Saint Petersburg State University
Saint Petersburg
Russian Federation
st040077@student.spbu.ru

Article history:
Received 01.12.2023, Accepted 26.12.2023

Abstract

In the present study, machine learning algorithms are applied for modeling transport coefficients in strongly nonequilibrium reacting gas flows. As a model case, the problem of a high-speed flow of a five-component air mixture around a sphere is considered. Various approaches for an application of machine learning methods, such as linear regression, k-nearest neighbors, support vector machine, regression tree, random forest, gradient boosting, and neural network (multilayer perceptron) are investigated. For the transport coefficients regression modelling the combination of machine learning methods with the finite volume method is constructed. The machine learning regressors are trained on the accurate numerical data given by one-temperature approach of the kinetic theory. The results of trained models are compared with approximate formulae of Blottner-Eucken-Wilke model. The results of different machine learning methods are analyzed in terms of the relationship between the obtained accuracy of calculations and the overall speed of calculations. The overall time of dataset formation and model training is estimated. The design of the constructed multilayer perceptron is discussed. The machine learning methods considered in the article can be used for the engineering problem such as design of high-speed aircraft, as well as for modeling of flows around complex shape bodies.

Key words

Computational Gas Dynamics, Machine Learning (ML), Neural Networks (NN), Transport Coefficients, OpenFOAM

1 Introduction

In recent years, sharp increase in the implementation of machine learning methods for modeling of physical systems is detected [Fradkov, 2022; Plotnikov et al., 2019; Fradkov and Shepeljavyi, 2022; Knyazev et al., 2023]. One of the most contemporary engineering problem is the accurate modeling of non-equilibrium flow problems, and, in particular, high-speed flows [Schmidt et al., 2019; Stokes et al., 2020; Brunton et al., 2020; Istomin, 2023]. For high-velocity flows the effects of significant increase in temperature behind the leading shock wave, the shock-front blurring, deceleration of the flow within the shock layer, and aerodynamic heating of the surface are observed. These effects lead for the necessity to take into account physical and chemical processes, such as an excitation of internal degrees of freedom (in particular, vibrational and electronic), as well as dissociation and ionization processes, and state-to-state reactions. The processes mentioned above, along with the reduction in gaseous medium density during high-altitude flight, may have a significant impact on the flow [Surzhikov, 2011; Surzhikov, 2018; Dobrov et al., 2022].

In the case of a sufficiently high concentration of gas particles (Knudsen number $Kn \ll 1$), the classical model of a continuous medium can be used for the flow modelling. This model is based on the hydrodynamic equations obtained from the kinetic equations for the distribution function [Lunev, 2007; Nagnibeda and Kustova, 2009]. The systems of equations obtained in this case rarely allow an analytical solution, and therefore the use of numerical methods is usually required [Anderson, 2019]. These problems tends for the modelling with the use of approximate formulae, that are typically applicable within a limited range of gas-dynamic parameters. It is obvious that such an approach cannot be treated as flexible one due to impossibility of using for the conditions outside the limited range of such approximation.

The approximation of a subset of the complete system of gas dynamics equations for computational fluid mechanics problems are widely studied [Ihme et al.,

2009; Tracey et al., 2015; Sun et al., 2019]. For a different specific issues, such as developing of a simplified neural network model as an algebraic turbulence model for computational fluid dynamics (CFD) simulation [Sun et al., 2019]; a data-driven approach to turbulence modeling in Reynolds-averaged Navier–Stokes (RANS) simulations leveraging supervised learning algorithms to improve the accuracy of turbulence closure terms in CFD simulations [Tracey et al., 2015]; large-eddy simulations (LES) for a methane-hydrogen flame modelling [Ihme et al., 2009], etc.; the machine learning methods are applied.

An overview of various applications of machine learning methods in fluid and gas mechanics can be found in [Brunton et al., 2020]. In the paper [Campoli, 2021], within the framework of the relaxation problem behind a direct shock wave, the use of regression algorithms for finding relaxation terms in kinetic equations, as well as the use of a deep neural network for approximation of the solution of the complete system of ideal gas equations, are considered. In the work [Weiner et al., 2019] the use of such fusion for calculation optimization for the problem of modelling transport processes in the boundary layer via preliminary trained neural network on a model problem is presented. The possibility of accelerating the calculation using a neural network model on a coarser grid, maintaining the required accuracy, is shown. The implementation of a combination of the finite volume method and data analysis tools at each computational step for hydroaeromechanics problems are shown in [Maulik et al., 2022].

Machine learning methods offer a promising alternative to exact computational schemes by achieving accurate parameter calculations specified during the training stage in a significantly shorter computational time. Such an approach for numerical simulation problems gives a clear computational advantage. Moreover, using of an input vector that defines the parameters of the flow, allows to save the dependencies of the output data on the input parameters. Currently, such methods has been started to be actively used in the field of modern gas dynamics. The implementation of machine learning methods for accurate prediction pf physical quantities via processing of large amounts of available data leads to a significant reduction of computational effort and allows for implementation for detailed state-resolved physical-chemical kinetics models, relaxation rates and transport coefficients [Istomin and Kustova, 2021; Campoli et al., 2022; Bushmakova and Kustova, 2022; Gorikhovskii and Kustova, 2022].It is shown that both approaches are promising for further implementation in simulation problem. The use of a neural network trained on the data of transport coefficients calculated by the methods of kinetic theory, is investigated in [Istomin and Kustova, 2021]. It is shown that neural networks make it possible to obtain a significant acceleration of the calculation speed for the transport coefficients, especially for gas mixtures: the potential acceleration in calculation speed increases as the number of gas mixture species rises [Istomin and Kustova, 2021]. In our last investigation [Pavlov and Istomin, 2023] it is shown that among several machine learning methods (neural network, linear regression, k-nearest neighbours, and support vector machines), neural network regression is the most flexible and promising method in terms of computational speed and precision. In the present study the following list of methods is supplemented by widely used methods such as regression tree, random forest and gradient boosting. Additionally to this, the comparison between different neural network architectures with varying number of layers and neurons is discussed.

In the present study the application of machine learning methods to the problem of a high-speed air flow around a sphere as a model simulation is considered. It is assumed that air consists of a five-component mixture (N_2, N, O_2, O, NO), taking into account internal degrees of freedom of the molecules (rotational and vibrational). Ionization effects are not considered in this study, as far as our primary focus is on the possibility for implementation of various machine learning methods. The initial conditions of the simulation align with those of the experiment [Lobb, 1964]. The experiment provides experimental data on the thickness of the shock layer, which can be measured using optical methods. This thickness is exceptionally responsive to the underlying physical and chemical processes behind the shock wave. The experiment covers a wide range of flow velocities (2400-6500 m/s), approximately corresponding to the initial condition of the reentry spacecraft into the Earth's atmosphere. Additionally, the experiment is often used for validation of the numerical simulation of high-speed flows [Surzhikov, 2011; Dobrov et al., 2022]. Refined experiment results for the velocity range (2500-3900 m/s) is given in [Nonaka et al., 2000]. Velocities around 9800 m/s are discussed in [Zander et al., 2014].

The work seeks for the following objectives: the first section describes the mathematical model of high-speed flow. In the second section computational model for the accurate and approximate approaches of transport coefficients calculation are considered. The third section covers the generation of the training dataset and the application of machine learning methods based on the accuracy and calculation time benchmarks. Finally, the results and recommendations for the most suitable machine learning methods, from the computational point of view, are provided.

2 Theoretical model of a viscous reacting gas mixture flow

For high-speed flows of reacting gases many phenomena that are not typical for supersonic flow are indicated [Anderson, 2019]. These phenomena include the thinning of the shock layer and the expansion of the boundary layer. Consequently, they can merge into a viscous shock layer, which requires the need of viscos-

ity calculation for simulation issue. As a result, classical gas-dynamic equations are inadequate for the flow description [Anderson, 2019]. At the same time high temperatures just behind the shock front lead to energy dependence on the mixture composition. that may changes due to chemical reactions, excitation of the internal degrees of freedom of species, ionization etc. Concluding this, in case of accurate modeling for gas dynamics problem all the effects mentioned above have to be taken into account.

Under strongly non-equilibrium conditions multi-temperature model or a state-to-state model are preferable to be applied [Nagnibeda and Kustova, 2009]. At the present work we consider continuum approximation, assuming that the rotational and translational energy modes of all species can be described by a single temperature T_{tr}; vibrational and electronic energy modes of all species supposed to be described by a single temperature T_{ve}. The discussion on the validity of such an approach can be found in [Scalabrin, 2007].

Under such an assumptions, the governing equations for a viscous reacting multi-component gas have the following form [Scalabrin, 2007]:

$$\frac{\partial \mathcal{U}}{\partial t} + \frac{\partial (\mathcal{F}_{i,inv} - \mathcal{F}_{i,vis})}{\partial x_i} = \dot{\mathcal{W}}, \tag{1}$$

where the vector of conservative variables $\mathcal{U}$ is presented in the form:

$$\mathcal{U} = \left(\rho,\, \rho_s,\, \rho u,\, \rho v,\, \rho w,\, E_{ve,s},\, E\right)^T, \tag{2}$$

$$s = N_2, N, O_2, O, NO$$

here u, v, w are the velocity components, ρ is the gas mass density, ρ_s is the partial density of the s-species. The flux density vector is divided into inviscid and viscous parts (diffusion and convective fluxes, respectively):

$$\mathcal{F}_{i,inv} = \begin{pmatrix} \rho u_i \\ \rho_s u_i \\ \rho u_i u + \delta_{i1} p \\ \rho u_i v + \delta_{i2} p \\ \rho u_i w + \delta_{i3} p \\ E_{ve,s} u_i \\ E u_i + p u_i \end{pmatrix}, \tag{3}$$

$$\mathcal{F}_{i,vis} = \begin{pmatrix} 0 \\ 0 \\ \tau_{i1} \\ \tau_{i3} \\ \tau_{i3} \\ -q_{ve,i,s} \\ \tau_{ij} u^j - q_{tr,i} - q_{ve,i} \end{pmatrix}, \tag{4}$$

$$\dot{\mathcal{W}} = \left(0,\, \dot{\omega}_s,\, 0,\, 0,\, 0,\, 0\right)^T, \tag{5}$$

here $E_{ve,s}$ is the total vibrational-electronic energy per unit volume of mixture of the s-species in the mixture (in particularly, only electronic in case of atomic species), δ_{ij} is the Kronecker symbol, $\dot{W}$ is the source term vector, $\dot{\omega}_s$ is a source term of the s-species due to chemical reactions. For the calculation stability, continuity equations for the overall mass density and the density of each components are solved simultaneously and independently.

The pressure p is restored by partial components according to the Dalton's law:

$$p = \sum_s p = \sum_s (\rho_s R_s T_{tr}) \tag{6}$$

here R_s is the specific gas constant corresponding to the s species.

The total energy per unit volume can be expressed in the following form:

$$E = \frac{1}{2}\rho(u^2+v^2+w^2) + E_t + \sum_s E_{ve,s} + \sum_s \rho_s h_s^o, \tag{7}$$

here h_s^0 is the tabulated enthalpy for the s-species [Scalabrin, 2007], $E_t = E_{tr} + E_{rot}$ is the summ of energies of translational and rotational degrees of freedom over all species in the mixture, $E_{ve,s} = E_{v,s} + E_{e,s}$ is the summ of energies of vibrational and electronic degrees of freedom for s-species. The specific energies of different degrees of freedom for molecular species are calculated by the following relations:

$$e_{t,s} = \frac{3}{2} R_s T_{tr}, \tag{8}$$

$$e_{r,s} = R_s T_{tr}, \tag{9}$$

$$e_{v,s} = R_s \frac{\theta_{v,s}}{e^{\theta_{v,s}/T_{ve}} - 1}, \tag{10}$$

$$e_{el,s} = R_s \frac{\sum\limits_{i \neq 0} g_{i,s} \theta_{el,i,s} e^{-\theta_{el,i,s}/T_{ve}}}{\sum\limits_{i} g_{i,s} e^{-\theta_{el,i,s}/T_{ve}}}, \tag{11}$$

here $\theta_{v,s}$ is the characteristic vibrational temperature for the s-species, $\theta_{el,i,s}$ and $g_{i,s}$ are the characteristic electronic temperature and the degeneracy of the energy level i for s-species. In the present study, five and four low-lying electronic energy levels of atomic N and O are taken into account; for molecular species $N_2,\ O_2,\ NO$ there are 15, 7, and 16 electronic levels, that are taken into account [Scalabrin, 2007].

Table 1. Initial conditions of experiments

Initial conditions	Values
Sphere diameter, D	0.0127 m (0.5 inches)
Velocity, v_∞	experiment #1: 2438 m/s
	experiment #2: 6051 m/s
Density, ρ_∞	7.9 g/m^3
Temperature, T_∞	293 K
Initial gas mixture	$N_2(76.6\%)$, $O_2(23.4\%)$

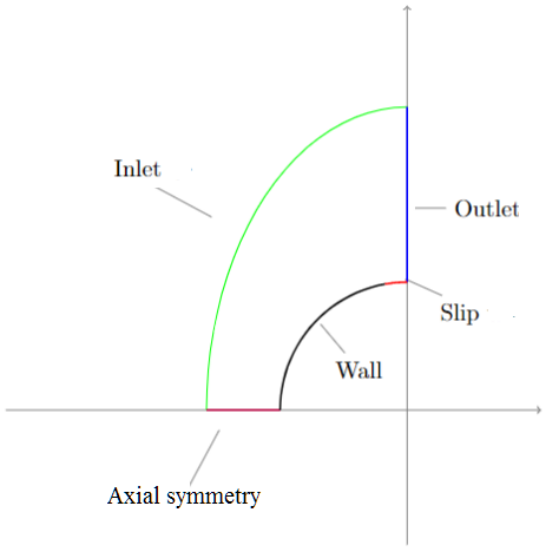

Figure 1. Computational domain in the projection on the meridional plane.

Table 2. List of accounted chemical reactions.

#	Reaction
1.	$O_2 + M \rightleftharpoons 2O + M$
2.	$N_2 + M \rightleftharpoons 2N + M$
3.	$NO + M \rightleftharpoons N + O + M$
4.	$NO + O \rightleftharpoons O_2 + N$
5.	$N_2 + O \rightleftharpoons NO + N$

Using expressions (8)-(11), the specific enthalpies at constant volume for each species can be expressed [Scalabrin, 2007]:

$$C_{v_{t,s}} = \frac{3}{2}R_s, \tag{12}$$

$$C_{v_{r,s}} = R_s, \tag{13}$$

$$C_{v_{v,s}} = R_s \frac{(\theta_{v,s}/T_{ve})^2 e^{\frac{\theta_{v,s}}{T_{ve}}}}{\left(e^{\frac{\theta_{v,s}}{T_{ve}}} - 1\right)^2}, \tag{14}$$

$$C_{v_{el,s}} = \frac{\partial e_{el,s}}{\partial T_{ve}}, \tag{15}$$

According to the law of mass action, the right hand side of the equation (1) for source term $\dot{\omega}_s$ of the s-species due to chemical reactions can be calculated:

$$\dot{\omega}_s = M_s \sum_s (\nu''_{s,r} - \nu'_{s,r}) \times$$

$$\left[k_{f,r} \prod_s \left(\frac{\rho_k}{M_k}\right)^{\nu'_{k,r}} - k_{b,r} \prod_s \left(\frac{\rho_k}{M_k}\right)^{\nu''_{k,r}}\right], \tag{16}$$

here $\nu'_{s,r}, \nu''_{s,r}$ are the stoichiometric coefficients of the direct and reverse reactions of the s-species in the reaction r, the summation occurs over all reactions.

Rate constant of a chemical reaction k_f satisfies the Arrhenius law:

$$k_f(T_{c,f}) = A \times T_{c,f}^{\beta} \exp\left(-\frac{T_a}{T_{c,f}}\right), \tag{17}$$

here A and β are the frequency factor and specific constant of each reaction [Scalabrin, 2007], T_a is the activation temperature, $T_{c,f}$ is the effective temperature of the forward reaction. For backward reactions the rate coefficient is calculated by the formula:

$$k_{b,r} = \frac{k_{f,r}}{K_r}, \tag{18}$$

here K_r is the equilibrium constant.

2.1 High-speed flow past a sphere

The principal scheme of the high-speed flow around a sphere according to an experiment [Lobb, 1964] is given in the Figure 1. In the experiment, a small diameter nylon sphere is fired into the air using a light-gas launcher. With a photographic setup and an optical schlieren system, the shock detachment distance was captured and measured over a wide range of high-speed velocities. In the present study two initial conditions #1 and #2 behind the shock front are considered (see Table 1).

When modeling, a five-component airflow, consisting of (N_2, N, O_2, O, NO), is considered. In the Table 2 The list of accounted reactions of dissociation (reactions 1-3) and Zeldovich reactions (reactions 4 and 5) is presented.

Reaction rate constants are taken from well known Park's model [Park, 1993]. For dissociation reaction the effective temperature changes according to Park's model [Park, 1990]:

$$T_P = T_{tr}^{\alpha_P} \times T_{ve}^{1-\alpha_P}, \tag{19}$$

here $\alpha_P = 0.7$ [Candler and Nompelis, 2009]. For Zeldovich reactions T_{tr} is used.

For numerical simulations of high-speed viscous flows under two-temperature approach, it is necessary to solve equations (1)–(4) for each volume of the computational grid, while the grid size may reaches millions of cells or even more, depending on the flow geometry. For this reason implementation of machine learning methods for many various engineering issues like transport coefficients calculation may crucially increase the speed up and overall precision.

3 Transport coefficients modelling

Taking into account the Stokes hypothesis, the components of the viscous stress tensor τ_{ij} in the equation (4) have the following form:

$$\tau_{ij} = \eta\Big(\frac{\partial u_i}{\partial x_j} + \frac{\partial u_j}{\partial x_i}\Big) + (\zeta + \eta_2)\frac{\partial u_k}{\partial x_k}\delta_{ij}, \qquad (20)$$

here η and ζ are shear and bulk viscosity coefficients, $\eta_2 = \zeta - \frac{2}{3}\eta$ is second viscosity coefficient. In the further modelling the Stokes hypothesis is stated: $\zeta = 0,\ \ \eta_2 = -\frac{2}{3}\eta$.

3.1 Kinetic theory approach

In case of exact calculation of transport coefficients, the kinetic theory algorithms have to be implemented [Nagnibeda and Kustova, 2009]. Using Chapman-Enskog method, for two-temperature approach the first-order distribution function is derived in terms of the gradients of macroscopic flow parameters: velocity, temperatures, and species number densities. The relations for first-order distribution functions consist coefficients at the gradients that are unknown functions of molecular velocity. The integral equations for the unknown functions mentioned above are derived. Finally, the transport coefficients are expressed in terms of the bracket integrals with respect to the aforementioned unknown functions.

This means that at each calculation step of our modeling, linear systems of equations for each transport properties have to be solved numerically [Istomin et al., 2023]. It is worth noting that the order of linear systems depends on the chosen approach: the case of two-temperature approach, considered in the following work, represents one of simpler choice for high-speed flows [Istomin et al., 2022]. In this case, contrary to the most accurate state-to-state approach where the order of system ranges from several tens to several thousands, the number of linear equations remains around ten. Additionally, the transport coefficients represent functions of temperatures, pressure and number densities of all species, Consequently, even in two-temperature approach the problem of accurate calculation of transport coefficients remains a computational heavy task [Istomin et al., 2022]. It is worth mentioning that these rigorous computationally expensive algorithms are implemented in the $KAPPA$ library [Campoli et al., 2019] and $PAINeT$ software package [Istomin and Kustova, 2021].

In the present study, for assessment of our approach on applicability of machine learning methods, we are limited the calculation of thermal conductivity λ and shear viscosity η coefficients in a (N_2, N, O_2, O, NO) mixture by one-temperature approach, given in the dataset [Istomin, 2023]. Nevertheless, in the future work another databases, formed on the results of transport coefficients, given by two-temperature or state-to-state approaches, also can be easily implemented.

Due to the fact that training data are produced for one temperature approach, all the output data are calculated for single overall temperature. This overall temperature can be determined by considering the different molecular temperatures and their respective degrees of freedom [Butler and Brokaw, 1957]:

$$T = \frac{\sum_s X_s\left((\zeta_{t,s} + \zeta_{r,s})T_{tr} + (\zeta_{v,s} + \zeta_{e,s})T_{ve,s}\right)}{\sum_s X_s(\zeta_{t,s} + \zeta_{r,s} + \zeta_{v,s} + \zeta_{e,s})}, \qquad (21)$$

here ζ is the number of degrees of freedom in relation to one specific energy mode:

$$\zeta_{t,s} = 3, \qquad \zeta_{r,s} = 2,$$

$$\zeta_{v,s} = \frac{2c_{v,s}(T_{ve,s})}{R_s T_{ve,s}}, \qquad \zeta_{e,s} = \frac{2c_{el,s}(T_{ve,s})}{R_s T_{ve,s}}. \qquad (22)$$

3.2 Approximate formulae

The most computationally efficient and simple approach is implementation of approximate formulae like the Sutherland or Blottner equations for viscosity, and the Eucken equation for thermal conductivity relations [Eucken, 1913; Vincenti and Kruger, 1965; Blottner et al., 1971; Istomin et al., 2014]. Shear viscosity is calculated for each species in the mixture using the Blottner model [Blottner et al., 1971]:

$$\eta_s = 0.1e^{[(A_s \ln T_{tr} + B_s)\ln T_{tr} + C_s]}, \qquad (23)$$

A_s, B_s, C_s are tabulated constants [Scalabrin, 2007].

The spatial components of translational-rotational and vibrational-electronic thermal conductivity can be calculated by the Fourier law:

$$q_{tr,i} = -\lambda_{tr,s}\frac{\partial T_{tr,s}}{\partial x_i}, \quad q_{ve,i} = -\lambda_{ve,s}\frac{\partial T_{ve,s}}{\partial x_i}, \ \ s \in N_s. \qquad (24)$$

The thermal conductivity coefficients for each species are calculated taking into account the Eucken correction [Vincenti and Kruger, 1965]:

$$\lambda_s = \lambda_{tr,s} + \lambda_{ve,s}, \qquad (25)$$

Table 3. Machine learning algorithms and optimal hyperparameters

Algorithm	Optimal parameters
Linear regression	with intercept
k-nearest neighbors	number of neighbors: 70
Support vector machine	C: 2000, ε : 0.1
Regression tree	depth: up to 30 number of leaf nodes: up to 1000 min. sample number to split: 20
Random forest	depth: up to 70 minimum number to split: 2 number of trees: 400
Gradient boosting	learning rate : 0.05 depth: up to 5 number of trees: 1000 min. sample number to split: 10
Neural network (multilayer perceptron)	number of hidden layers: 1 number of neurons per layer: 64 activation function: ReLU optimizer: l-bgfs

$$\lambda_{tr,s} = \eta_s \left(\frac{5}{2} C_{v_{t,s}} + C_{v_{r,s}} \right), \qquad \lambda_{ve,s} = \frac{5}{4} \eta_s C_{v_{ve,s}},$$

here $C_{v_{t,s}}$, $C_{v_{r,s}}$, and $C_{v_{ve,s}}$ are the specific heats of translational, rotational, and vibrational-electronic degrees of freedom at a constant volume.

Thermal conductivity and shear viscosity coefficients for the mixture can be calculated using the Wilke's law [Wilke, 1950]:

$$\lambda = \sum_s \frac{X_s \lambda_s}{\phi_s}, \qquad \eta = \sum_s \frac{X_s \eta_s}{\phi_s}, \qquad (26)$$

here X_s is the mole fraction of the s species; $\lambda_s = \lambda_{tr,s} + \lambda_{ve,s}$; ϕ_s is the coefficient calculated as follows [Palmer and Wright, 2003]:

$$\phi_s = X_s + \sum_{r \neq s} X_r \Big(1 + \sqrt{\frac{\eta_s}{\eta_r}} \Big(\frac{M_r}{M_s} \Big)^{1/4} \Big)^2 \times$$

$$\times \Big(\sqrt{8 \Big(1 + \frac{M_s}{M_r} \Big)} \Big)^{-1}, \qquad r \in N_s, \qquad (27)$$

here M_s and M_r are the mass of the particles s and r, correspondingly.

It is worth to note that approximate formulae can be easily incorporated into engineering codes. However, these formulae are limited by the temperature and pressure ranges within they are valid, and are not intended for non-equilibrium conditions that occur in high-speed gas mixture flows. These considerations lead us to explore methods for accurately accounting for all effects, associated with high-speed non-equilibrium flows, as well as an efficient method for calculation of the transport coefficients taking into account all these effects.

3.3 Machine learning algorithms

To assess the usability of different machine learning algorithms, at the first step the transport coefficients of (N_2, N, O_2, O, NO) mixture are calculated using the $PAINeT$ (Planet Atmosphere Investigator of Non-equilibrium Thermodynamics) software package [Istomin, 2018; Istomin, 2019; Istomin and Kustova, 2021]. Another possible way is to use a simpler approach like Wilke's mixing rule, but with an accurate data of transport coefficients of single-component gases (the results from $PAINeT$ for each component of the mixture are also extracted). In the present study both approaches to the problem are assessed. It total, output vectors for the physical properties and transport coefficients $[C_p, \lambda_{tr}, \lambda_{int}, \eta]$ for six gases (5 single-component gases and (N_2, N, O_2, O, NO) and mixture) in wide ranges of input vector $[T, p, n_s]$ randomly generated values of temperature 273 - 100 000 K, pressure 500 - 202650 Pa, and number densities n_s are produced. The dataset, given in [Istomin, 2023], is used for training of different machine learning models.

The input vector of five-component mixture includes temperature, pressure, and molar fractions of mixture species, resulting in totally 7 features for each target variable (2 features for one-component gases). The dataset contains 30000 samples of these features for each coefficient. The validation of data is confirmed by the rigorous kinetic theory algorithms and experimental data [Istomin and Kustova, 2017]. Using the grid search algorithm and cross-validation procedure, the optimal parameters of various machine learning regression algorithms, presented in scikit-learn library [Pedregosa et al., 2011], are tuned. The list of the machine learning methods and optimal parameters are listed in the Table 3. For support vector machine and gradient boosting methods a multi-output wrapper of multi-target regression is implemented. For neural network (multilayer perceptron model) the rectified linear unit (*ReLU*):

$$f(x) = max(0, x),$$

as an activation function is implemented.

The dataset is split into training and test sets, with proportions of 70% and 30%, respectively. All input data are normalized with z-score normalization. Using the different loss functions: mean absolute procentage error (MAPE) and root mean square error (RMSE), as well as the coefficient of determination (R^2), the comparison on the test samples after training procedure is produced. The evaluation of the trained models is made on the whole test set. Furthermore, comparison of computational times for training and a sample output vector prediction using the selected optimal model is provided.

Table 4. Comparison of accuracy metrics for multicomponent air regression on the output vector $[C_p, \eta, \lambda_{tr}, \lambda_{int}]$

Algorithm	MAPE	RMSE	R^2
Linear regression	0.3339	0.578	0.6773
k-nearest neighbors	0.1223	0.350	0.8808
Support vector machine	0.0118	0.109	0.9885
Regression tree	0.0357	0.189	0.9654
Random forest	0.0070	0.084	0.9932
Gradient boosting	0.0023	0.047	0.9978
Neural network	0.0072	2.0e-6	0.9999

Table 5. Comparison of training t_{learn} and prediction t_{pred} times for multicomponent air regression on the output vector $[C_p, \eta, \lambda_{tr}, \lambda_{int}]$

Algorithm	$t_{learn}, [s]$	$t_{pred}, [s]$	$\frac{t_{learn}}{t_{pred}}$
Linear regression	0.005	0.0002	33
k-nearest neighbors	0.006	0.1587	0.04
Support vector machine	818.5	0.5323	1537
Regression tree	0.041	0.0003	137
Random forest	30.78	0.4126	75
Gradient boosting	103.3	0.1770	584
Neural network	11.58	0.1505	77

3.4 Application of neural network to CFD simulation

At the first stage, CFD flow simulation is carried out according to the model proposed in Section 2. After that, on the basis of calculated transport coefficients, using the values of pressures and temperatures on the stagnation line the regression model of trained neural network is applied. Pressure, temperatures and molar fraction values, obtained through CFD simulation, are used as input data for the regression models. Finally, all the results for different models and approaches are compared between each other: 1) approximate formulae implementation (Blottner-Eucken-Wilke model): 2) neural network regressor of output vector for the mixture; and 3) neural networks regressor of output vector for the single-component gas with further implementation of Wilke's mixing rule.

4 Results

4.1 Evaluation of machine learning methods applicability

The results on the accuracy and calculation times for the different machine learning algorithms are presented in the Tables 4 and 5. Various approaches for an application of machine learning methods, such as linear regression, k-nearest neighbors, support vector machine, regression tree, random forest, gradient boosting, and neural network (multilayer perceptron) are investigated. Conventional statistical methods for regression problem are unable to effectively handle complex interactions within the dataset, whereas machine learning algorithms generally demonstrate satisfactory accuracy level (with exception of k-nearest neighbors and linear regression algorithms). At the same time we have to keep in mind, that all these algorithms are limited by the requirement of large datasets for effective model training. Based on the obtained results, the most promising in terms of the accuracy and speed of calculation is neural network (multilayer perceptron model). Ensemble methods like gradient boosting and random forest also demonstrate good accuracy; however, they both require significantly more computational resources for training and execution (see Table 5). The $t_{learn}/t_{predict}$ ratio here serves as a metric to assess the efficiency trade-off between the learning and prediction stages, offering insights into resource utilization and scalability: lower values provides the potential for retraining or fine-tuning the model.

4.2 Optimal neural network regression model

As soon as the speed-up and accuracy of the multilayer perceptron with a one-hidden-layer architecture for output vector modeling, as stated in the subsection above, are confirmed, another interesting question arises: what is the relationship between the optimal computation time (minimum number of neurons and/or layers required) and the desired level of accuracy? Comparison between different neural network architectures with varying number of layers and neurons is shown in the Table 6 for different accuracy metrics, and in the Table 7 for the training and prediction calculation times. It is clearly seen, that the lowest error metrics and best value of the coefficient of determination R^2 belongs to two architectures of 64 and (32, 32) neurons in the hidden layer(s). Further in the present study the architecture of 64 neurons in one-hidden layer multilayer perceptron model is implemented. Nevertheless, it is worth to note that neural network architectures, deeper than three hidden layers, also may have greater potential after meticulous study for hyperparameter selection.

The comparison in Tables 6 and 7 also includes the evaluation of different neural network architectures in terms of metric results and calculation times. It is observed that when comparing neural network regression with approximate formulae, the latter becomes an ineffective choice in terms of accuracy, even when computational speed is comparable. It must be noticed, that given value for prediction calculation time of approximate formulae is the result of vectorized and optimized code realization for computation fluid dynamic solver, while for neural network regression optimization is built in into the code from scratch [Pedregosa et al., 2011]. For such realizations the speed-up up to 4 times for best neural network regressor is detected.

Table 6. Comparison of accuracy metrics for different multulayer perceptron architecture.

Perceptrons in layers	MAPE	MAE	MSE	R^2
4	5e-02	1e-05	3e-10	0.99395
32	9e-03	2e-06	5e-12	0.99989
64	7e-03	1e-06	3e-12	0.99992
(4, 4)	3e-02	9e-06	1e-10	0.99706
(16, 16)	7e-03	2e-06	4e-12	0.99991
(32, 32)	7e-03	1e-06	3e-12	0.99992
(8, 8, 8)	1e-02	3e-06	2e-11	0.99964
(16, 16, 16)	1e-02	2e-06	9e-12	0.99979
(32, 32, 32)	6e-03	2e-06	5e-12	0.99989
Approximate formulae	8e-02	4e-05	4e-09	0.91462

Table 7. Comparison of training t_{learn} and prediction t_{pred} times for different types of multulayer perceptron architecture.

Perceptrons in layers	$t_{learn}, [s]$	$t_{pred}, [s]$	$\frac{t_{learn}}{t_{pred}}$
4	5.38	0.011	489
32	9.19	0.071	129
64	11.58	0.151	77
(4, 4)	5.90	0.019	31
(16, 16)	9.96	0.056	18
(32, 32)	12.59	0.145	87
(8, 8, 8)	11.41	0.056	204
(16, 16, 16)	15.97	0.108	148
(32, 32, 32)	17.41	0.223	78
Approximate formulae	-	0.526	-

Once the model is configured and trained, the neural network's weight array and configuration data can be transferred as a surrogate model to external CFD solvers [Jiang2020]. This approach holds promising potential for enhancing accuracy and accelerating computational speed in CFD solvers when simulating viscous high-speed nonequilibrium reacting flows.

4.3 Neural network implementation for transport coefficients calculation

The behavior of temperatures T, T_{tr}, and T_{ve} behind the shock front is shown on the Figure 2. For the experiments [Lobb, 1964], considered in the study, Mach numbers are approximately equal to 9 and 20, and therefore just behind the shock front temperature grows sharply and reaches 5 000 K and 10 000 K correspondingly.

On the Figures 3 and 4 the comparison of the results for shear viscosity η (see Figure 3) and thermal conductivity λ (see Figure 4), given by different models, are shown.

For direct application of the regression model we consider the different options of regressions of transport coefficients: regression for the mixture, or regression of individual components with the Wilke's mixing rule. The comparison of the different approaches for the shear viscosity calculation (see Figure 3) shows, that before the shock wave all the models for shear viscosity calculations are nearly coincide (discrepancy does not exceed 5-10 %), while just behind the shock front the maximum of mean absolute percentage error may achieved up to 40 %.

Following equation (25) for approximate formulae, thermal conductivity depends on shear viscosity, and therefore its behavior (see Figure 4) is very similar for those presented on Figure 3. The one difference is that for thermal conductivity the results for Eucken model and Wilke's rule for neural network results are overestimated results for mixture, given by the accurate results of neural network.

The results above are confined by the relative errors presented in Table 8, which shows the average and maximum absolute percentage errors for shear viscosity (η) and thermal conductivity (λ). These values are calculated using the Blottner-Eucken-Wilke model and single-component neural networks with Wilke's mixing rule.

Under such strongly non-equilibrium conditions it is clearly seen that approximate Blottner model overestimates the values of shear viscosity in the high-temperature range just behind the shock front. In contrast, implementation of Eucken formulae underestimates thermal conductivity coefficient. Additionally, it is shown, that implementation of neural networks for single-component gas with Wilke's mixing rule, strongly differs on both approximate and neural network for mixture models, and therefore, should not be employed in practical simulations.

Table 8. Average and maximum absolute percantage error of experiments #1 and #2 for shear viscosity η and thermal conductivity λ behind the shock front for Approximative model (Blottner and Eucken) and Neural network with Wilke's mixing rule, comparing to the most accurate data of Neural network for mixture

Experiment	**Approximate model, avg.**	**Approximate model, max.**	**Neural network (Wilke's rule), avg.**	**Neural network (Wilke's rule), max.**
η, #1	3.8%	18.3%	11.0%	43.1%
η, #2	9.8%	18.4%	23.6%	43.7%
λ, #1	16.4%	23.1%	14.3%	65.5%
λ, #2	17.8%	34.4%	31.8%	66.7%

5 Conclusion

In the present study, assessment of different machine learning methods for regression of transport coefficients is given. As a model case, the problem of a high-speed

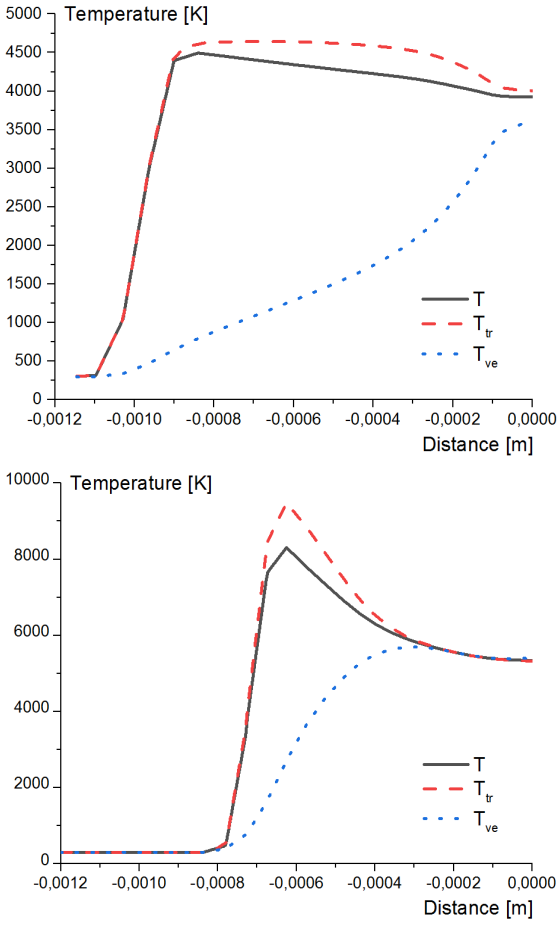

Figure 2. Behaviour of temperatures T, T_{tr}, T_{ve} behind the shock front for experiments #1 (top) and #2 (bottom).

flow of a five-component air mixture around a sphere is considered. Various approaches for an application of machine learning methods, such as linear regression, k-nearest neighbors, support vector machine, regression tree, random forest, gradient boosting, and neural network (multilayer perceptron) are investigated.

The machine learning regressors are trained on the accurate numerical data given by one-temperature approach of the kinetic theory. The results of trained models are compared with approximate formulae by the Blottner-Eucken-Wilke model.

The results of different machine learning methods are analyzed in terms of the relationship between the achieved accuracy of calculations and the speed of calculations. It is shown that neural networks regression is the most promising way in terms of achieving the desired precision while maintaining efficient calculation speed. Additionally, the comparison between different neural network architectures with varying number of layers and neurons is provided. The best architecture in terms of accuracy and computational efficiency is given. Approximate formulae of vectorized and optimized code realization for computation fluid dynamic solver, and neural network regression, given from scratch [Pedregosa et al., 2011], are compared. For such realizations the speed-up up to 4 times for best neural network regressor is detected.

It has been observed that, before the shock wave, the approximate formulae of the Blottner-Eucken-Wilke model and the application of neural network regressors yield qualitatively similar results, with a mean absolute percentage error falling in the range of 5-10%. However, just behind the shock front, the use of a mixing rule tends to overpredict the shear viscosity and thermal conductivity coefficients, resulting in a mean absolute percentage error of up to 40

This suggests that the utilization of neural network regression, specifically a multilayer perceptron, for modeling the vector of transport coefficients, including the diffusion coefficient (to be explored in future work), can potentially enhance computational efficiency for issues related to computational fluid dynamics. The methods discussed in this article are applicable to engineering problems such as high-speed aircraft design and modeling flows around complex-shaped bodies.

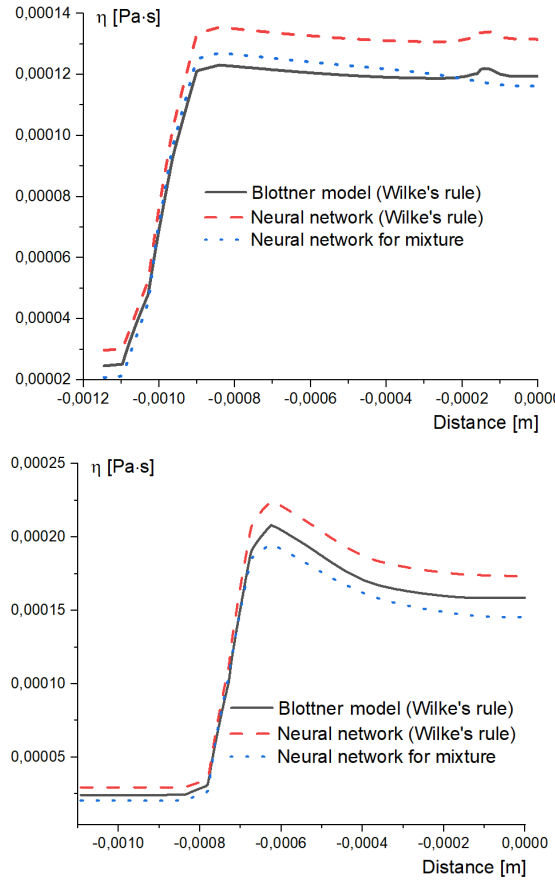

Figure 3. Shear viscosity coefficients behavior of different models as a function of distance behind the shock front for experiments #1 (top) and #2 (bottom).

Acknowledgements

The work is supported by Russian Science Foundation (project 23-29-00055).

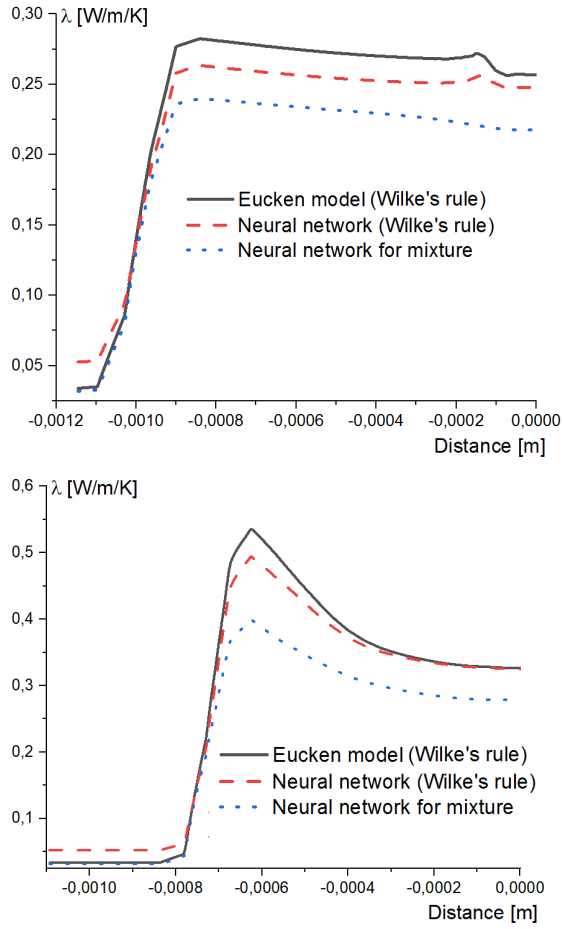

Figure 4. Thermal conductivity coefficients behaviour of different models as a function of distance behind the shock front for experiments #1 (top) and #2 (bottom).

References

Anderson, J. D. (2019). *Hypersonic and High-Temperature Gas Dynamics, Third Edition*. American Institute of Aeronautics and Astronautics, Inc.

Blottner, F. G., Johnson, M., and Ellis, M. (1971). Chemically reacting viscous flow program for multicomponent gas mixtures. techreport sc-rr-70-754, Albuquerque, New Mexico.

Brunton, S. L., Noack, B. R., and Koumoutsakos, P. (2020). Machine learning for fluid mechanics. *Annual Review of Fluid Mechanics*, **52** (1), pp. 477–508.

Bushmakova, M. and Kustova, E. (2022). Modeling the vibrational relaxation rate using machine-learning methods. *Vestnik St.Petersb. Univ.Math.*, **55**, pp. 87–95.

Butler, J. and Brokaw, R. (1957). Thermal conductivity of gas mixtures in chemical equilibrium. *J. Chem. Phys.*, **26**, pp. 1636.

Campoli, L. (2021). Machine learning methods for state-to-state approach. *AIP Conference Proceedings*, **2351** (1), pp. 030041.

Campoli, L., Kustova, E., and Maltseva, P. (2022). Assessment of machine learning methods for state-to-state approach in nonequilibrium flow simulations. *Mathematics*, **10** (6), pp. 1–21.

Campoli, L., Oblapenko, G., and Kustova, E. (2019). Kappa: Kinetic approach to physical processes in atmospheres library in c++. *Computer Physics Communications*, **236**, pp. 244–267.

Candler, G. V. and Nompelis, I. (2009). Computational fluid dynamics for atmospheric entry. RTO-EN-AVT-162.

Dobrov, Y., Gimadiev, V., Karpenko, A., and Volkov, K. (2022). Numerical simulation of hypersonic flow with non-equilibrium chemical reactions around sphere. *Acta Astronautica*, **194**, pp. 468–479.

Eucken, E. (1913). Ueber das Wärmeleitvermogen, die Spezifische Wärme und die innere Reibung der Gase. *Physik. Zeitschr*, **14**, pp. 324–332.

Fradkov, A. L. (2022). Cybernetics and physics: Ten years online together. *Cybernetics and Physics*, **11**, pp. 4–5.

Fradkov, A. L. and Shepeljavyi, A. I. (2022). The history of cybernetics and artificial intelligence: a view from Saint Petersburg. *Cybernetics and Physics*, **11**, pp. 253–263.

Gorikhovskii, V. I. and Kustova, E. V. (2022). Neural-network-based approach to the description of vibrational kinetics of carbon dioxide. *Vestnik St. Petersb. Univ. Math.*, **55**, pp. 434–442.

Ihme, M., Schmitt, C., and Pitsch, H. (2009). Optimal artificial neural networks and tabulation methods for chemistry representation in les of a bluff-body swirl-stabilized flame. *Proceedings of the Combustion Institute*, **32** (1), pp. 1527–1535.

Istomin, V. (2023). *Database for using of transport coefficients of atoms and molecules in gas dynamics problems (FSAMHD)*. Number 2023621081. Certificate of state registration of the database.

Istomin, V. and Kustova, E. (2017). Transport coefficients and heat fluxes in non-equilibrium high-temperature flows with electronic excitation. *Physics of Plasmas*, **24** (2), pp. 022109.

Istomin, V. and Kustova, E. (2021). Painet: Implementation of neural networks for transport coefficients calculation. *Journal of Physics: Conference Series*, **1959** (1), pp. 012024.

Istomin, V., Kustova, E., and K.A.Prutko (2022). Heat and radiative fluxes in strongly nonequilibrium flows behind shock waves. *Vestnik of Saint Petersburg University. Series 1. Mathematics. Mechanics. Astronomy*, **55** (4), pp. 461–470.

Istomin, V., Kustova, E., Lagutin, S., and Shalamov, I. (2023). Evaluation of state-specific transport proper-

ties using machine learning methods. *Cybernetics and Physics*, **12** (1), pp. 34–41.

Istomin, V. A. (2018). Painet: An object-oriented software package for simulations of flow-field, transport coefficients and flux terms in non-equilibrium gas mixture flows. *AIP Conference Proceedings*, **1959** (1), pp. 060006.

Istomin, V. A. (2019). Painet: Similarity criteria and different approaches of kinetic theory. *AIP Conference Proceedings*, **2132**, pp. 130005.

Istomin, V. A., Kustova, E. V., and Mekhonoshina, M. A. (2014). Eucken correction in high-temperature gases with electronic excitation. *J. Chem. Phys.*, **140**, pp. 184311.

Knyazev, N., Pershin, A., Golovkina, A., and Kozynchenko, V. (2023). Forecasting the state of complex network systems using machine learning methods. *Cybernetics and Physics*, (Volume 12, 2023, Number 2), pp. 129–135.

Lobb, R. K. (1964). Experimental measurement of shock detachment distance on spheres fired in air at hypervelocities. *High Temperature Aspects of Hypersonic Flow*, pp. 519–527.

Lunev, V. (2007). *Real gases flows of high velocities (in Russian)*. M.: Fizmatlit.

Maulik, R., Fytanidis, D. K., Lusch, B., Vishwanath, V., and Patel, S. (2022). Pythonfoam: In-situ data analyses with openfoam and python. *Journal of Computational Science*, **62**, pp. 101750.

Nagnibeda, E. and Kustova, E. (2009). *Nonequilibrium Reacting Gas Flows. Kinetic Theory of Transport and Relaxation Processes*. Springer-Verlag, Berlin, Heidelberg.

Nonaka, Satoshi, Mizuno, Hiroyasu, Takayama, Kazuyoshi, and Park, C. (2000). Measurement of shock standoff distance for sphere in ballistic range. *Journal of Thermophysics and Heat Transfer*, **14** (2), pp. 225–229.

Palmer, G. E. and Wright, M. J. (2003). Comparison of methods to compute high-temperature gas viscosity. *Journal of Thermophysics and Heat Transfer*, **17** (2), pp. 232–239.

Park, C. (1990). *Nonequilibrium hypersonic aerothermodynamics*. New York: Wiley.

Park, C. (1993). Review of chemical-kinetic problems of future nasa missions. i - earth entries. *Journal of Thermophysics and Heat Transfer*, **7** (3), pp. 385–398.

Pavlov, S. and Istomin, V. (2023). Application of machine learning methods to numerical simulation of hypersonic flow. *Moscow University Physics Bulletin*, **78** (1), pp. 180–187.

Pedregosa, F., Varoquaux, G., Gramfort, A., Michel, V., Thirion, B., Grisel, O., Blondel, M., Prettenhofer, P., Weiss, R., Dubourg, V., et al. (2011). Scikit-learn: Machine learning in python. *Journal of machine learning research*, **12** (Oct), pp. 2825–2830.

Plotnikov, S. A., Lipkovich, M., Semenov, D. M., and Fradkov, A. L. (2019). Artificial intelligence based neurofeedback. *Cybernetics and Physics*, **8**, pp. 287–291.

Scalabrin, L. C. (2007). *Numerical simulation of weakly ionized hypersonic flow over reentry capsules.* PhD thesis, The University of Michigan.

Schmidt, J., Marques, M. R. G., Botti, S., and Marques, M. A. L. (2019). Recent advances and applications of machine learning in solid-state materials science. *npj Computational Materials*, **5** (1), pp. 1–36.

Stokes, P. W., Casey, M. J. E., Cocks, D. G., de Urquijo, J., García, G., Brunger, M. J., and White, R. D. (2020). Self-consistent electron–THF cross sections derived using data-driven swarm analysis with a neural network model. *Plasma Sources Science and Technology*, **29** (10), pp. 1–10.

Sun, L., An, W., Liu, X., and Lyu, H. (2019). On developing data-driven turbulence model for dg solution of rans. *Chinese Journal of Aeronautics*, **32** (8), pp. 1869–1884.

Surzhikov, S. (2011). *Computational study of aerothermodynamics of hypersonic flow around blunt bodies using the example of experimental data analysis (in Russian)*. M.: IPMech RAS.

Surzhikov, S. (2018). *Computational aerophysics of descent space vehicles. 2D Models*. M.: Fizmatlib.

Tracey, B., Duraisamy, K., and Alonso, J. (2015). A machine learning strategy to assist turbulence model development. *53rd AIAA Aerospace Sciences Meeting*, pp. 1–22.

Vincenti, W. and Kruger, C. (1965). *Introduction to Physical Gas Dynamics*. Wiley.

Weiner, A., Hillenbrand, D., Marschall, H., and Bothe, D. (2019). Data-driven subgrid-scale modeling for convection-dominated concentration boundary layers. *Chemical Engineering I& Technology*, **42** (7), pp. 1349–1356.

Wilke, C. R. (1950). A viscosity equation for gas mixtures. *The Journal of Chemical Physics*, **18** (4), pp. 517–519.

Zander, F., Gollan, R. J., Jacobs, P. A., and Morgan, R. G. (2014). Hypervelocity shock standoff on spheres in air. *Shock Waves*, **24** (2), pp. 171–178.